iScience

CellPress
OPEN ACCESS

Article

MircroRNA-92b as a negative regulator of the TGF-β signaling by targeting the type I receptor

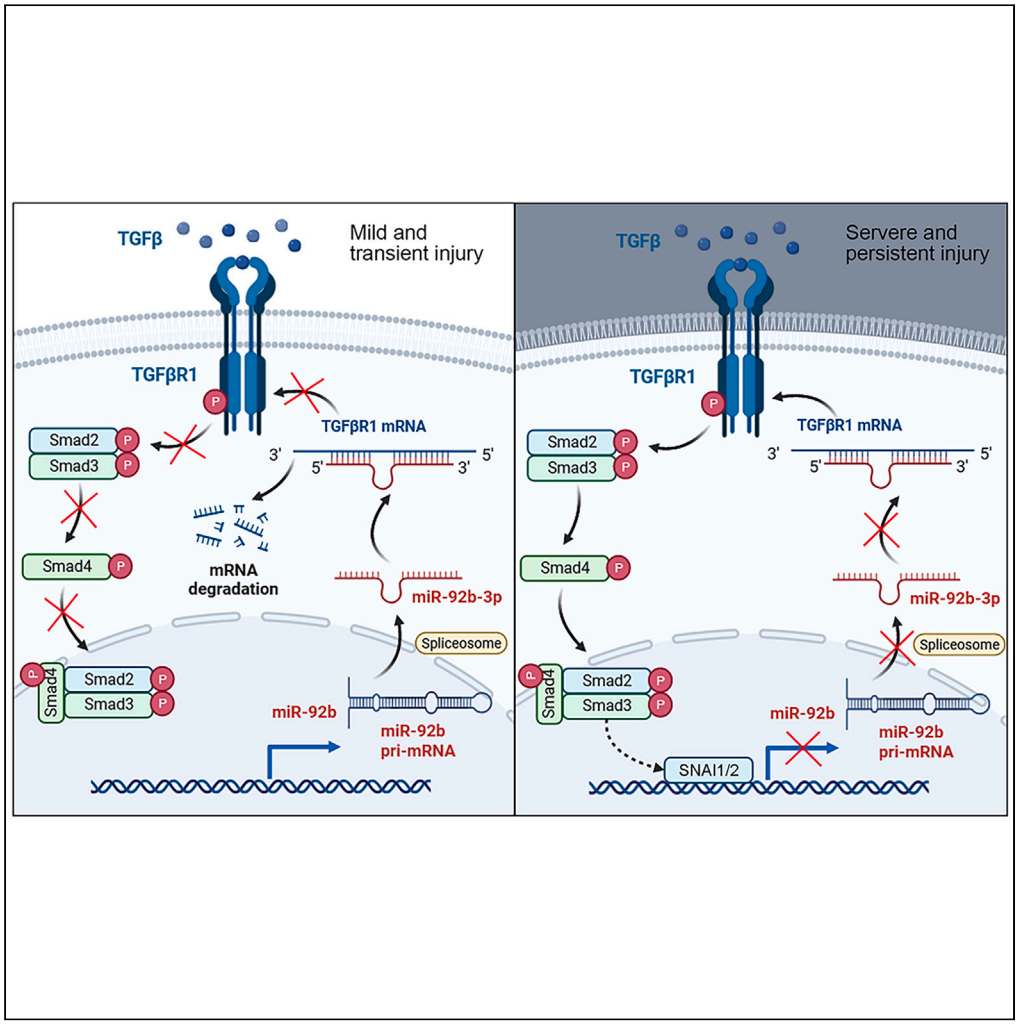

Shu Yang, Kewei Jiang, Lixing Li, ..., Lin Kang, Guangyan Yang, Zhen Liang

kang.lin@szhospital.com (L.K.)
guangyanyang0919@163.com (G.Y.)
liang.zhen@szhospital.com (Z.L.)

Highlights

MiR-92b knockout aggravates kidney fibrosis

MiR-92b overexpression protects from kidney fibrosis

MiR-92b-3p inhibits TGF-β signaling pathway by directly targeting TGF-β receptor 1

TGF-β suppresses miR-92b transcription through SNAI1 and SNAI2

Yang et al., iScience *26*, 108131
November 17, 2023
https://doi.org/10.1016/j.isci.2023.108131

iScience

CellPress
OPEN ACCESS

Article

MircroRNA-92b as a negative regulator of the TGF-β signaling by targeting the type I receptor

Shu Yang,[1,2,4] Kewei Jiang,[1,2,4] Lixing Li,[1,2,4] Jiaqing Xiang,[1,2] Yanchun Li,[1,2] Lin Kang,[1,2,3,*] Guangyan Yang,[1,2,*] and Zhen Liang[1,2,5,*]

SUMMARY

Transforming growth factor β1 (TGFβ1) has been identified as a major pathogenic factor underlying the development of chronic kidney disease (CKD). This study investigated the role of miR-92b-3p in the progression of renal fibrosis in unilateral ureteral occlusion (UUO) and unilateral ischemia-reperfusion injury (uIRI) mouse models, as well as explored its underlying mechanisms in human proximal tubular epithelial (HK2) cells. We found that renal fibrosis increased in UUO mice after miR-92b knockout, while it reduced in miR-92b overexpressing mice. MiR-92b knockout aggravated renal fibrosis in uIRI mice. RNA-sequencing analysis, the luciferase reporter assay, qPCR analysis, and western blotting confirmed that miR-92b-3p directly targeted TGF-β receptor 1, thereby ameliorating renal fibrosis by suppressing the TGF-β signaling pathway. Furthermore, we found that TGF-β suppressed miR-92b transcription through Snail family transcriptional repressors 1 and 2. Our results suggest that miR-92b-3p may serve as a novel therapeutic for mitigating fibrosis in CKD.

INTRODUCTION

Renal fibrosis is a common pathological characteristic of almost all progressive chronic kidney diseases (CKDs), including diabetic kidney disease (DKD) and obstructive nephropathy,[1,2] and its process greatly diminishes the regenerative potential of the kidneys, leading to decreased function.[3] Currently, there is no approved treatment for renal fibrosis. Therefore, an improved understanding of the cellular and molecular mechanisms of renal fibrosis is paramount and essential for not only gaining novel insights into the pathogenesis of the process but also developing rational strategies to treat patients with fibrotic kidney disorders.[4]

Transforming growth factor β (TGF-β) plays a pivotal role in chronic inflammatory changes of the interstitium and accumulation of ECM during renal fibrogenesis.[5] Emerging evidence suggests that TGF-β initiates the transition of renal tubular epithelial cells to myofibroblasts, the cellular source for ECM deposition, leading ultimately to an irreversible renal failure.[6] Inhibition of the TGF-β isoform, TGF-β1, or its downstream signaling pathways substantially limits renal fibrosis in a wide range of disease models, whereas TGF-β1 overexpression induces renal fibrosis.[7] TGF-β1 can induce renal fibrosis via activation of both canonical (Smad-based) and non-canonical (non-Smad-based) signaling pathways, which result in the activation of myofibroblasts, excessive production of the ECM, and inhibition of ECM degradation.[8] The activated SMAD complex enters the nucleus and transcribes fibrosis-associated proteins, such as type I collagen (COL1A1) and smooth muscle actin (SMA).[9] SMAD3 requires phosphorylation for nuclear translocation and transcriptional regulation of the target genes in fibrosis.[10] Studies over the past 5 years have identified additional mechanisms, including short and long non-coding RNA molecules and epigenetic modifications of DNA and histone proteins, that regulate TGF-β1/Smad signaling in fibrosis.[7]

Small non-coding RNAs serve a wide range of regulatory roles and have increasingly been recognized as therapeutic targets.[11] One of the best-studied classes of small non-coding RNAs is microRNAs (miRNAs) which can act as master regulators of gene expression.[12] They have a length of approximately 18–25 nucleotides and regulate important cellular processes by inhibiting gene expression through the post-transcriptional repression of target mRNAs.[13,14] In kidneys, miRNAs have been associated with renal development, homeostasis, and physiological functions.[15] Clinical and experimental animal studies have revealed that miRNAs play essential roles in the pathogenesis of various renal diseases.[16] Emerging evidence demonstrate the relationship between TGF-β signaling and miRNA expression during renal diseases.[17] For

[1]Department of Geriatrics, Shenzhen People's Hospital (The Second Clinical Medical College, Jinan University; The First Affiliated Hospital, Southern University of Science and Technology), Shenzhen 518000, China
[2]Guangdong Provincial Clinical Research Center for Geriatrics，Shenzhen Clinical Research Center for Geriatrics, Shenzhen People's Hospital (The Second Clinical Medical College, Jinan University; The First Affiliated Hospital, Southern University of Science and Technology), Shenzhen, 518000 China.
[3]The Biobank of National Innovation Center for Advanced Medical Devices, Shenzhen People's Hospital, Shenzhen 518000, China
[4]These authors contributed equally
[5]Lead contact
*Correspondence: kang.lin@szhospital.com (L.K.), guangyanyang0919@163.com (G.Y.), liang.zhen@szhospital.com (Z.L.)
https://doi.org/10.1016/j.isci.2023.108131

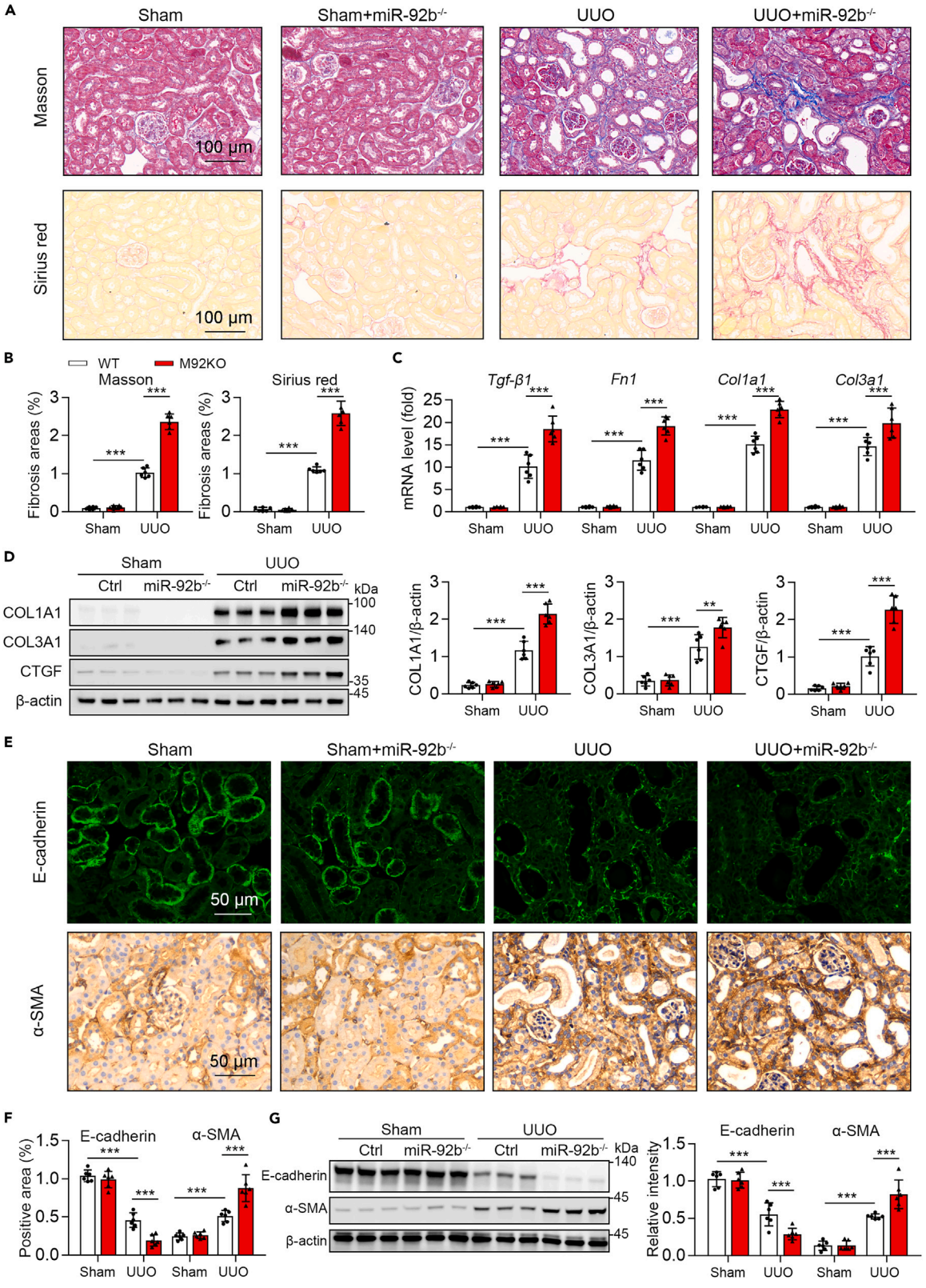
A
Sham
Sham+miR-92b-/-
UUO
UUO+miR-92b-/-
Masson
Sirius red
100 μm
B
WT
M92KO
Masson
Sirius red
Fibrosis areas (%)
Sham
UUO
C
Tgf-β1
Fn1
Col1a1
Col3a1
mRNA level (fold)
D
Sham
UUO
Ctrl
miR-92b-/-
kDa
COL1A1
COL3A1
CTGF
β-actin
COL1A1/β-actin
COL3A1/β-actin
CTGF/β-actin
E
E-cadherin
α-SMA
50 μm
F
Positive area (%)
G
Relative intensity

Figure 1. Global knockout of miR-92b aggravated renal fibrosis in UUO mic

(A and B) Representative images of Masson's trichrome staining for tubulointerstitial fibrosis and collagen deposition (blue), and Sirius red staining in kidney sections from WT and miR-92b knockout mice at day 7 post surgery (A); Scale bar: 100 μm. Quantitative analysis of fibrotic area as determined by Masson's trichrome staining (the left panel) and Sirius red staining (the right panel) (B); n = 6.

(C) qPCR analysis of mRNA levels of *Tgfb*, *Fn1*, *Col1a1*, and *Col3a1*.

(D) Western blotting analysis of COL1A1, COL3A1, CTGF, and β-actin; quantitative results are shown in the right panel. β-actin was used as the loading control; n = 6.

(E and F) Representative images of E-cadherin immunofluorescence staining and immunohistochemistry for α-SMA in renal tissue (E), and quantitative analysis of positive area (F); Scale bar: 50 μm; n = 6.

(G) Western blotting of E-cadherin, α-SMA, and β-actin; quantitative results shown in the right panel.β-actin was used as the loading control. Data are expressed as means ± SD; n = 6. *p < 0.05, **p < 0.01, ***p < 0.001.

instance, miR-192 has been reported to be up-regulated in the glomeruli of type 1 and type 2 diabetic mice and cultured mesangial cells treated with TGF-β1 increased the expression of collagen 1a2 by down-regulating Zeb2, an E-box repressor.[18] Previous research has shown that miR-377 expression was up-regulated in mouse models of diabetic nephropathy and cultured human and mouse mesangial cells treated with high concentrations of glucose and TGF-β1.[19] Although the role of the TGF-β signaling pathway in mediating renal fibrosis is well established, the associated key microRNAs have not yet been elucidated.

It had been reported that the expression of miR-92b-3p was disorders in the kidney of DKD mice and rats.[20,21] Interestingly, the role of miR-92b on the progression of fibrosis seems contradictory. For instance, a study showed that miR-92b-3p promotes the activation of hepatic stellate cell and thereby the progression of liver fibrosis by activating JAK/STAT pathway via targeting CREB3L2.[22] In contrast, another study reported that peroxisome proliferator-activated receptor-γ-induced miR-92b expression inhibited Axl expression and in turn reduced expression of TGF-β1 and the downstream genes in keloid patients.[23] In addition, the role of miR-92b in the progress of renal fibrosis was remaining unknown. Hence, we investigated the role of miR-92b in the progression of TGF-β-mediated renal fibrosis and explored the underlying mechanisms in this study.

In this study, we identified the role of miR-92b-3p in renal fibrosis and observed that miR-92b-3p is significantly downregulated in mouse fibrotic kidneys. Mechanistically, we characterized miR-92b-3p as a key checkpoint for controlling TGF-β signaling and fibrogenesis. Global deletion of miR-92b-3p markedly aggravated the extent of renal fibrosis in fibrotic mouse kidney tissues induced by UUO and unilateral ischemia-reperfusion injury (uIRI). Importantly, we showed that renal TEC-specific overexpression of miR-92b-3p effectively ameliorated the development and progression of kidney fibrosis induced by UUO. Our findings suggest that targeting miR-92b-3p may be a novel and potential approach to treat renal fibrosis and preserve kidney function.

RESULTS

MiR-92b knockout aggravated kidney fibrosis in UUO mice

To investigate the potential involvement of miR-92b in the pathogenesis of kidney fibrosis, we first determined its expression levels in fibrotic mouse kidney tissue induced by UUO. The qPCR results showed significant downregulation of miR-92b-3p expression levels in fibrotic mouse kidneys (Figure S1A). Using datasets from the GEO database (GSE51674), we found that miR-92b-3p was downregulated in renal samples from patients with DKD who underwent kidney biopsy compared to normal controls (Figure S1B).

We first found that kidneys from M92KO mice (Figure S2A) displayed a similar kidney structure, kidney-to-body weight ratio, urinary albumin excretion rate, albumin-to-creatinine ratio, and 24 h urine volume to wild-type (WT) mice (Figures S2B and S2C). To determine the effects of miR-92b on the development of fibrosis in kidneys *in vivo*, WT and M92KO mice were challenged with UUO (Figures 1A and 1B). After UUO surgery, renal fibrosis was evident in kidney sections from WT mice (assessed by Sirius Red and Masson's trichrome staining; Figures 1A and 1B). In line with this, fibrogenic factor (*Tgf-β1, Fn1, Col1a1,* and *Col3a1*) expression was remarkably upregulated in the kidney of UUO mice (Figure 1C). Consistently, the protein levels of COL1A1, COL3A1, and CTGF were increased in WT mice after UUO (Figure 1D). Additionally, UUO surgery reduced E-cadherin accumulation while upregulating α-SMA accumulation in mouse kidney (Figures 1E–1G). Compared to WT mice, M92KO mice exhibited more evident renal fibrosis (Figures 1A and 1B). The M92KO mice also showed higher levels of *Tgf-β1, Fn1, Col1a1,* and *Col3a1* (Figure 1C), as well as, elevated levels of kidney COL1A1, COL3A1, CTGF, and α-SMA proteins and decreased levels of E-cadherin compared to WT mice (Figures 1D–1G). Therefore, the loss of miR-92b augmented the extent of kidney fibrosis in UUO mice.

MiR-92b knockout aggravated kidney fibrosis in uIRI mice

To further study the role of miR-92b in the development of renal fibrosis, WT and M92KO mice were subjected to uIRI. Compared to sham mice, renal fibrosis was evident in sections from uIRI mice, as assessed by Masson and Sirius red staining (Figures 2A–2C). Renal fibrosis was enhanced in M92KO mice compared to WT mice after uIRI surgery (Figures 2A–2C). Furthermore, uIRI surgery reduced E-cadherin accumulation and increased α-SMA accumulation in mouse kidneys, and these changes were augmented in M92KO than in WT mice (Figures 2D and 2E). Finally, the protein levels of COL1A1, COL3A1, and α-SMA (Figure 2F), as well as, the mRNA levels of *Col1a1, Col1a2, Col3a1, Fn1*, and *Ctgf* (Figure 2G) increased in mice after uIRI surgery, and these changes were enhanced in M92KO than in WT mice (Figures 2G and 2F). Taken together, these results indicate that the loss of miR-92b augmented the extent of kidney fibrosis in uIRI mice.

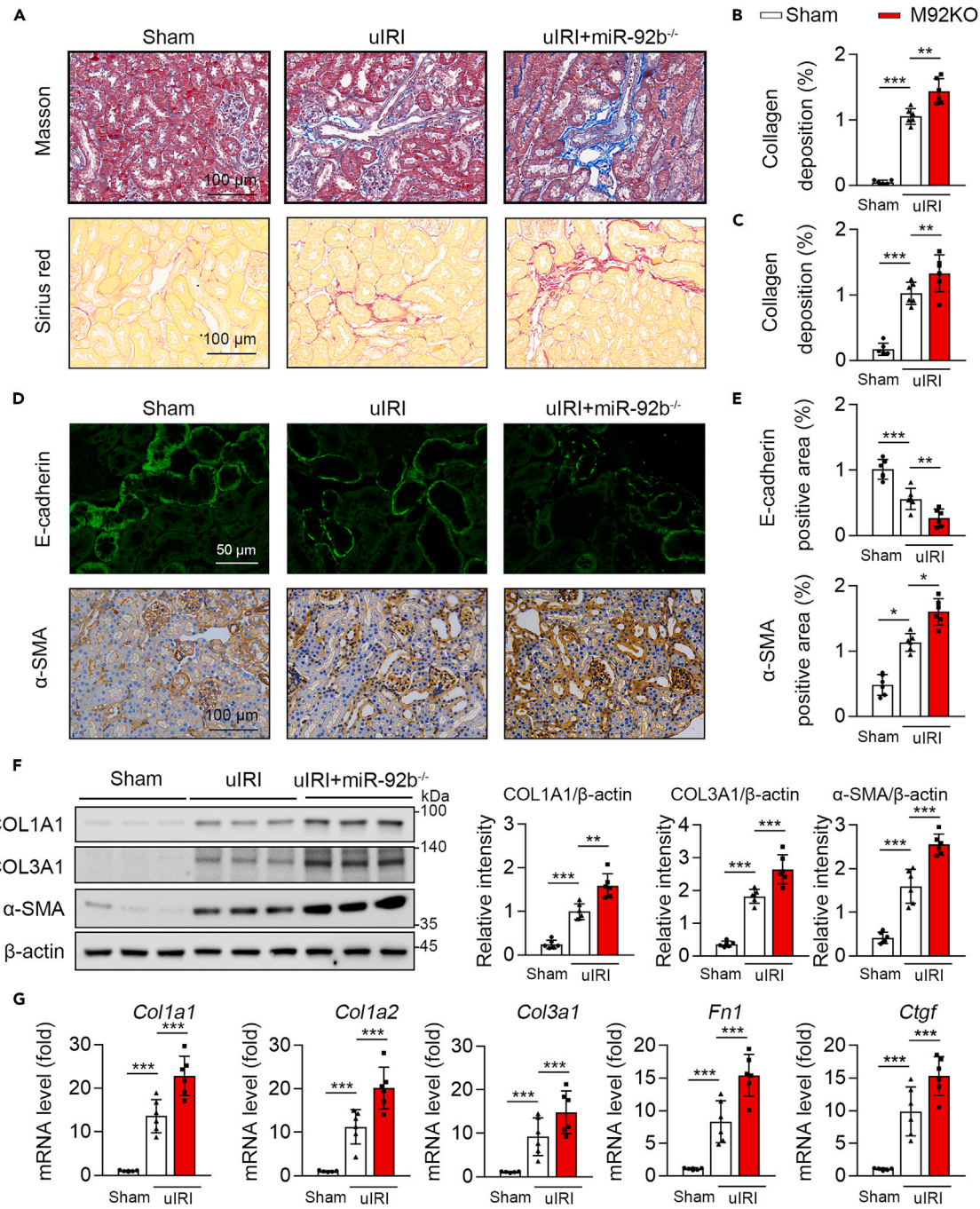

Figure 2. Global knockout of miR-92b aggravated renal fibrosis in uIRI mice

(A–C) Renal tissue samples were collected 24 days after renal ischemia-reperfusion (IR) or sham control surgery. Representative images of Masson's trichrome and Sirius red staining in kidney sections from WT and miR-92b knockout mice 24 days after surgery (A); Scale bar: 100 μm. Quantitative analysis of fibrotic area as determined by Masson's trichrome staining (B) and Sirius red staining (C); n = 6.

(D and E) Representative images of E-cadherin immunofluorescence staining and immunohistochemistry for α-SMA in renal tissue (D), and quantitative analysis of positive area (E); Scale bar: 50 μm; n = 6.

(F) Western blotting analysis of COL1A1, COL3A1, α-SMA, and β-actin; quantitative results are shown in the right panel. β-actin was used as the loading control actin; n = 6.

(G) qPCR analysis of mRNA levels of *Col1a1*, *Col1a2*, *Col3a1*, *Fn1*, and *Ctgf*. Data are expressed as means ± SD; n = 6. *p < 0.05, **p < 0.01, ***p < 0.001.

MiR-92b overexpression alleviated kidney fibrosis in UUO mice

Next, the opposing phenotypes were examined in mice overexpressing miR-92b. We then performed renal-specific overexpression of miR-92b in C57BL/6 mice by renal *in situ* injection of AAV9- miR-92b (M92OE) or AAV9- GFP (control group) at three independent to induce miR-92b overexpression, and UUO surgery was performed 2 weeks after the injection. Compared with the control group, M92OE mice showed reduced collagen deposition (assessed by Sirius red staining; Figures 3A and 3B), decreased E-cadherin loss (Figure 3C), reduced α-SMA accumulation (Figure 3C), decreased the protein levels of COL1A1, COL3A1, and α-SMA (Figure 3E), and down-regulated the mRNA levels of *Col1a1*, *Col1a2*, *Col3a1*, *Fn1*, and *Ctgf* (Figure 3F) in the kidney of UUO mice. Moreover, there is a significantly higher level of miR-92b-3p in the kidney of M92OE mice compared to those in control group (Figure 3G). These results suggest that MiR-92b overexpression in the kidney alleviates renal fibrosis in UUO.

MiR-92b-3p regulated the activation of the TGF-β signaling pathway

Differential gene expression analyses identified 1181 significantly upregulated and 950 significantly downregulated genes in the kidneys of M92KO mice compared to WT mice ($p < 0.05$; Figure 4A). Notably, ingenuity pathway analysis (IPA) revealed that the "TGF-β signaling pathway" was the top pathway affected by miR-92b knockout (Figures 4B and 4C). TGF-β is considered a master cytokine/growth factor produced within injured or diseased tissues, where it activates fibroblasts and facilitates ECM production.[24] TGF-β binds a heterodimeric receptor in the plasma membrane consisting of the TGF-β type I and type II half-receptors, which together induce phosphorylation of SMAD2 and SMAD3 transcription factors in mediating canonical signaling. Phosphorylated SMAD2 and SMAD3 interact with Smad4 in the cytoplasm, from where they translocate to the nucleus to induce gene transcription.[25] Importantly, both TGFBR1 and TGFBR2 were upregulated in the kidneys of M92KO mice compared to WT mice (Figures 4D and 4E).

Using TargetScan databases to predict the downstream targets of miR-92b-3p, 1292 downstream conserved target genes in humans and mice were predicted. Interestingly, IPA of 1292 genes revealed that "TGF-β Receptor Signaling" and "TGF-β receptor signaling in skeletal dysplasias" were the top pathways predicted by TargetScan (Figure 5A). Next, we found that miR-92b-3p was expressed more in HK2 cells than in mesangial cells (HMC), glomerular endothelial cells (HRGEC), and renal fibroblast cells (HRF) (Figure 5B). Hence, we next examined whether the activation of TGF-β signaling pathway was regulated by miR-92b in the HK2 cell line. We found that the phosphorylation of SMAD3 and expression of COL1A1 and α-SMA increased in HK2 cells under TGF-β stimulation, as measured by western blotting (Figures 5C and 5D). Moreover, we observed a decrease in SMAD3 phosphorylation and downregulation of COL1A1 and α-SMA by miR-92b mimic treatment in HK2 cells. In line with this, the expression of TGF-β target genes (*COL1A1* and *SERPINE1*) were upregulated by TGF-β stimulation, and these changes were prevented by miR-92b mimic treatment. However, *CDH1* (This gene encodes E-cadherin) was down-regulated by TGF-β stimulation, and was aggravated by miR-92b mimic treatment (Figure 5E). Moreover, nuclear SMAD3 localization induced by TGF-β stimulation was inhibited by miR-92b mimic treatment, as assessed by western blotting (Figure 5F). Furthermore, miR-92b inhibitor (miR-92bi) increased TGF-β-mediated the upregulation of SMAD3 phosphorylation, protein levels of COL1A1 and α-SMA, mRNA levels of *COL1A1* and *SERPINE1*, and the nuclear accumulation of SMAD3 (Figures 5G–5I). In line with this, miR-92b mimic treatment inhibited the TGF-β-induced phosphorylation of SMAD3 and the expression of TGF-β target genes in HRFs (human renal fibroblasts) (Figures S3A and S3B).

TGFBR1 is the direct target of miR-92b-3p

Using StarBase (http://starbase.sysu.edu.cn/), we identified TGFBR1 as a potential miR-92b target in both humans and mice (Figure 6A). MiR-92b mimic decreased mRNA levels of *TGFBR1* in a time- and dose-dependent manner compared to control RNA treatment in HK2 cells (Figure 6B). To further investigate the interaction between miR-92b and *TGFBR1*, we constructed two plasmids, TGFBR1 3′-UTR-WT and TGFBR1-3′-UTR-MT containing the WT and mutant of the 3′-UTR of TGFBR1, respectively. Each plasmid was co-transfected with miR-92b mimic into HK2 cells. miR-92b mimic treatment reduced the activity of luciferase reporters in a dose-dependent manner in cells transfected with TGFBR1 3′-UTR-WT, while had no evident effect on the activity of luciferase reporters those transfected with TGFBR1-3′-UTR-MT (Figure 6C). These results suggest that *TGFBR1* is a direct target mRNA of miR-92b-3p. Furthermore, we found that miR-92b mimic treatment restrained induced up-regulation of TGF-β-induced TGFBR1 in HK2 cells, whereas miR-92b inhibitor treatment augmented this change (Figure 6D). Next, to explore whether miR-92b regulates the activation of the TGF-β signaling pathway depending on TGFBR1, HK2 cells were treated with miR-92b inhibitor (miR-92bi) and siRNA *Tgfbr1* separately or in combination. *Tgfbr1* siRNA treatment decreased the phosphorylation of SMAD3 in HK2 cells in the presence of TGF-β, which did not further change after miR-92bitreatment (Figure 6E). In line with this, TGFBR1 knockdown suppressed TGF-β induced mRNA levels of α-SMA and COL1A1, which did not change after miR-92bitreatment (Figure 6F). In contrast, adenovirus-mediated *Tgfbr1* overexpression increased the phosphorylation of Smad3 (Figure 6G) and the mRNA levels of *a-SMA* and *COL1A1* (Figure 6H) in HK2 cells under TGF-β stimulation; these changes were not affected by miR-92b mimic treatment. Notably, miR-92b OE restrained the upregulation of *Tgfbr1* mRNA and protein levels in the kidneys of UUO mice, and miR-92b knockout enhanced these changes (Figure 6I). Taken together, miR-92b regulates TGF-β signaling pathway activation by inhibiting *Tgfbr1*exrepssion through directly binding to the 3′-UTR of *Tgfbr1*.

TGFBR1 deficiency suppressed the renal injury mediated by global deletion of miR-92b in UUO mice

We further determined whether the global knockout of miR-92b aggravated obstructive nephropathy through the renal ablation of TGFBR1 in mice. Compared with the control group, AAV9-*Ggt-shTgfbr1*-mediated renal tubular epithelium-specific TGFBR1 knockdown in UUO mice decreased collagen deposition (Figures 7A–7C), enhanced E-cadherin accumulation (Figure 7D), reduced the accumulation of α-SMA (Figure 7D), and decreased the protein levels of COL1A1, COL3A1, and α-SMA, as well as the mRNA levels of *Col1a1, Col1a2, Col3a1, Fn1*, and

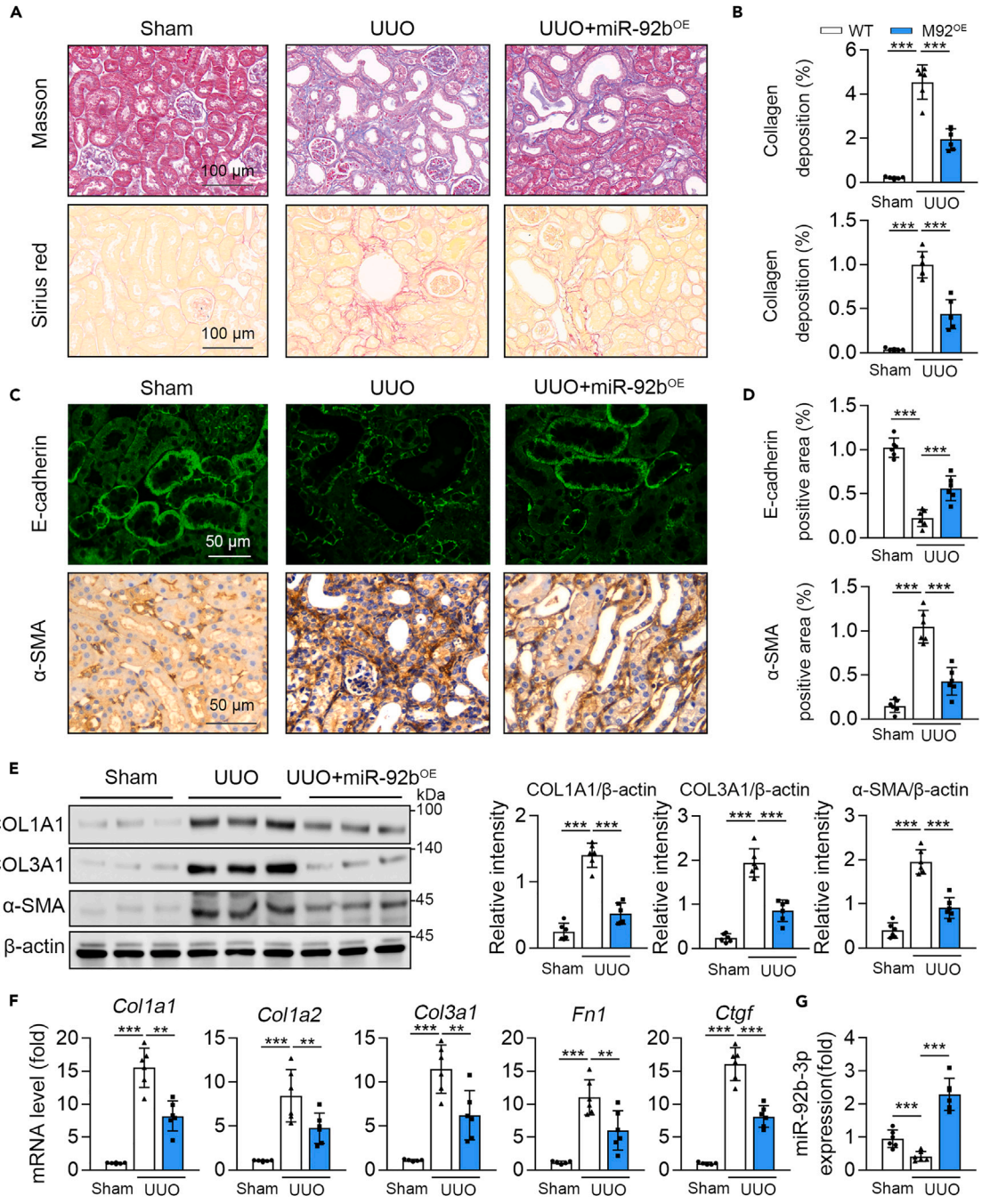

Figure 3. MiR-92b overexpression alleviated renal fibrosis in UUO mice

(A and B) Representative images of Masson's trichrome and Sirius red staining in kidney sections from WT and miR-92b OE mice at day 10 post surgery (A); Scale bar: 100 μm. Quantitative analysis of fibrotic area as determined by Masson's trichrome staining (B, the upper panel) and Sirius red staining (B, the bottom panel); n = 6.

(C and D) Representative images of E-cadherin immunofluorescence staining and immunohistochemistry for α-SMA in renal tissue (C), and quantitative analysis of positive area (D); Scale bar: 50 μm; n = 6.

(E) Western blotting of E-cadherin, α-SMA, and β-actin; quantitative results are shown in the right panel. β-actin was used as the loading control; n = 6.

(F) qPCR analysis of mRNA levels of *Col1a1*, *Col1a2*, *Col3a1*, *Fn1*, and *Ctgf*; n = 6.

(G) qPCR analysis of miR-92b-3p; n = 6. Data are expressed as means ± SD, n = 6. *p < 0.05, **p < 0.01, ***p < 0.001.

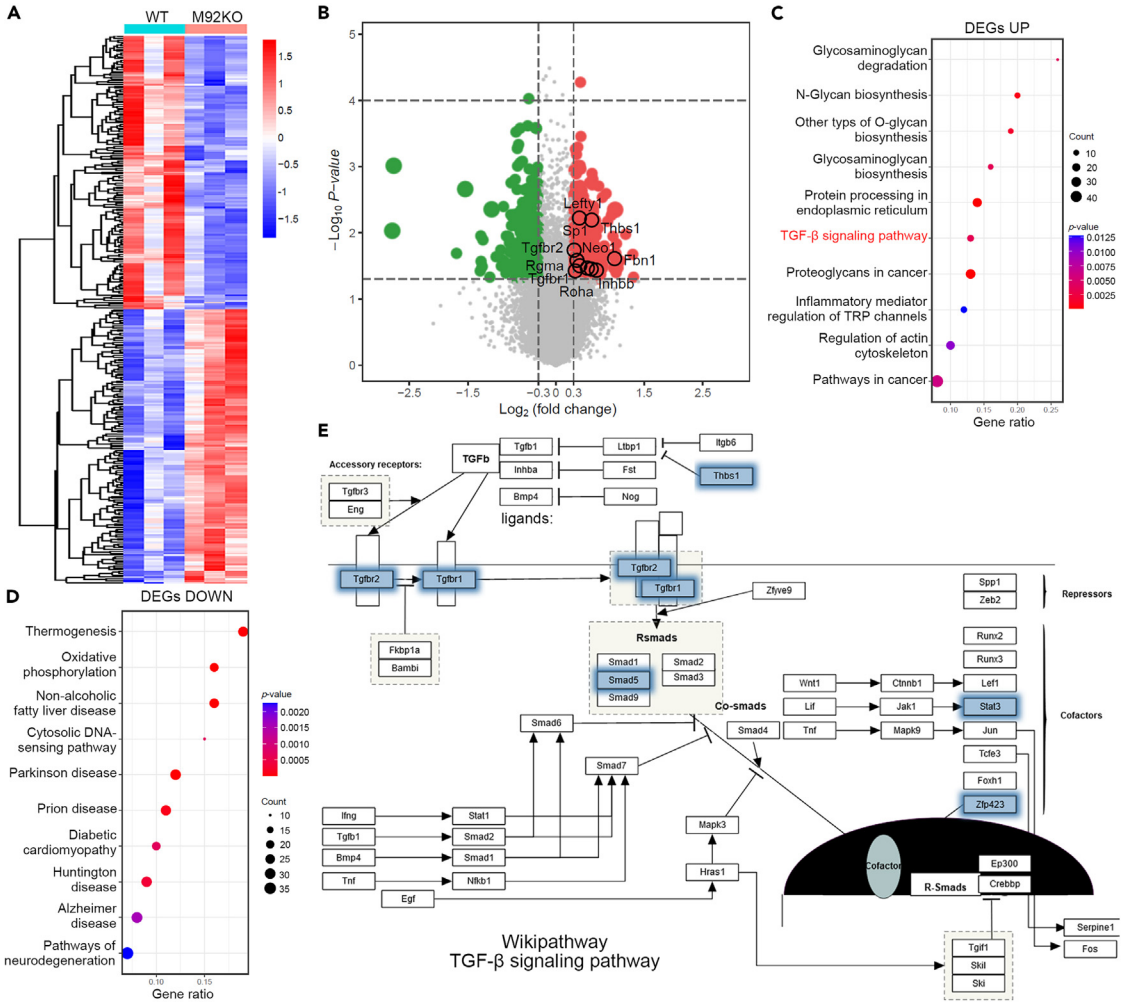

Figure 4. IPA predicts a strong regulation of TGF-β pathways by miR-92b in the kidneys of mice. (A to E) RNA-seq of kidney from M92KO and WT mice

(A) Heatmap of differentially expressed genes in the kidneys of M92KO and WT mice (n = 3).

(B) Volcano plot of differentially expressed genes in the kidneys of M92KO and WT mice (Downregulated: $p < 0.05$ and log FC < -0.3; Upregulated: $p < 0.05$ and log FC > 0.3). Genes related to the TGF-β signaling pathway are labeled.

(C and D) Ingenuity Pathway Analysis (IPA) of RNA-seq.

(E) Wikipathway of the TGF-β signaling pathway.

Ctgf (Figures 7F and 7G). However, there was no significant difference in collagen deposition or profibrogenic gene expression in the kidneys of miR-92b knockout UUO and WT mice after AAV-shTgfbr1 transfection. Overall, these data suggested that TGFBR1 is an important target of miR-92b in renal fibrosis.

SNAI1 and SNAI2 mediated TGF-β-induced suppression of miR-92b in HK2 cells

To explore the mechanisms underlying the decreased expression of miR-92b-3p in the fibrotic kidney, we first observed whether TGF-β1 regulates the expression of miR-92b-3p. We found that TGF-β stimulation suppressed the expression of miR-92b-3p in HK2 cells (Figure 8A). It had been reported that Snail Family Transcriptional Repressor 1 and 2 (SNAI1 and SNAI2) mediated TGF-β-induced suppression of E-cadherin.[26,27] SNAI1 and SNAI2 are transcription factors that share a similar DNA-binding structure with five C2H2 zinc finger motifs, which bind specifically to a subset of E-box motifs (E-box: CAGGTG/CACCTG) in target promoters, such as the E-cadherin promoter, and are key mediators of epithelial-to-mesenchymal transition (EMT) (Figure 8B).[26] As expected, the loss of SNAI1 or SNAI2 inhibited the TGF-β-induced downregulation of miR-92b-3p expression (Figures 8C and 8D). In addition, when both SNAI1 and SNAI2 were absent, the TGF-β treatment had no significant effect on the expression of miR-92b-3p (Figure 8E).

MiR-92b is located within thrombospondin 3 antisense RNA 1 (THBS3-AS1), and we found that there are two E-box sequences (E-box1: CACCTG; E-box2: CAGGTGACAGGTG) in the THBS3-AS1 primer; E-box1 is recognized by SNAI2 and E-box2 by both SNAI1 and SNAI2 (Figure 8F). Hence, we cloned a series of THBS3-AS1 promoter deletion mutants into the luciferase reporter system

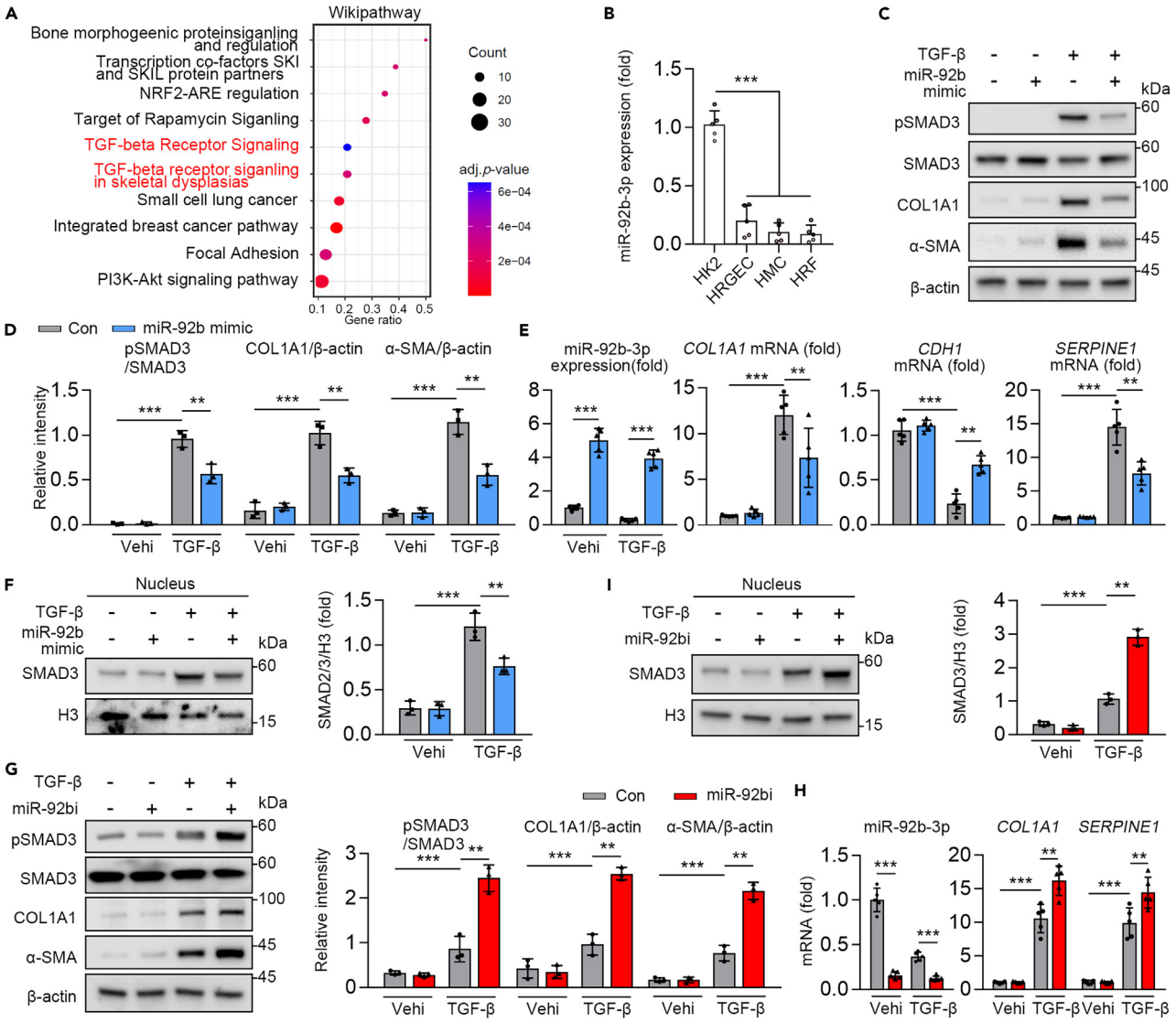

Figure 5. MiR-92b-3p regulated the activation of the TGF-β signaling pathway

(A) The Ingenuity Pathway Analysis (IPA) of the predicted target of miR-92b.

(B) The expression of miR-92b-3p in various cells; n = 5.

(C and D) Western blotting of phosphorylation of SMAD3 (*p*-SMAD3), SMAD3, COLL1A1, α-SMA, and β-actin in HK2 cells transfected with miR92b mimic for 24 h and treated with or without 2 ng/mL TGF-β for 24 h; quantitative results are shown in panel D; n = 3.

(E) qPCR analysis of the expression of miR-92b-3p and the mRNA levels of *COL1A1*, *CFH1*, and *SERPINE*1; n = 5.

(F) Western blotting of SMAD3 and H3 in the nuclear extract from HK2 cells transfected with miR-92b mimic for 24 h and treated with or without 2 ng/mL TGF-β for indicated times; quantitative results are shown in the right panel; n = 3.

(G) Western blotting of phosphorylation of SMAD3 (*p*-SMAD3), SMAD3, COL1A1, α-SMA, and β-actin in HK2 cells treated with miR-92b inhibitor (miR-92bi) and/or TGF-β (2 ng/mL) for 24 h; quantitative results are shown in the left panel; n = 3.

(H) qPCR analysis of the expression of miR-92b-3p and the mRNA levels of *COLL1A1* and *SERPINE*1; n = 5.

(I) Western blot analyses of SMAD3 and H3 in the nuclear extract from HK2 cells transfected with miR92b inhibitor and/or 2 ng/mL TGF-β for 24 h; quantitative results are shown in the middle panel, n = 3. Data are expressed as means ± SD; *p < 0.05, **p < 0.01, ***p < 0.001.

(Luc1–Luc3; Figure 8G) and found that overexpression of TGF-β suppressed THBS3-AS1 activity in the Luc1 and Luc2 constructs, indicating that the minimal SNAI1 or SNAI2 binding site within the THBS3-AS1 promoter was between −2,520 and −1,200 bp. We further performed chromatin immunoprecipitation (ChIP) assays and found that SNAI2 was recruited to the −2,224 to −2,113 bp region of the THBS3-AS1 promoter, while SNAI1 and SNAI2 were recruited to the −2016 bp to −1852 bp region of the THBS3-AS1 promoter (Figure 8H).

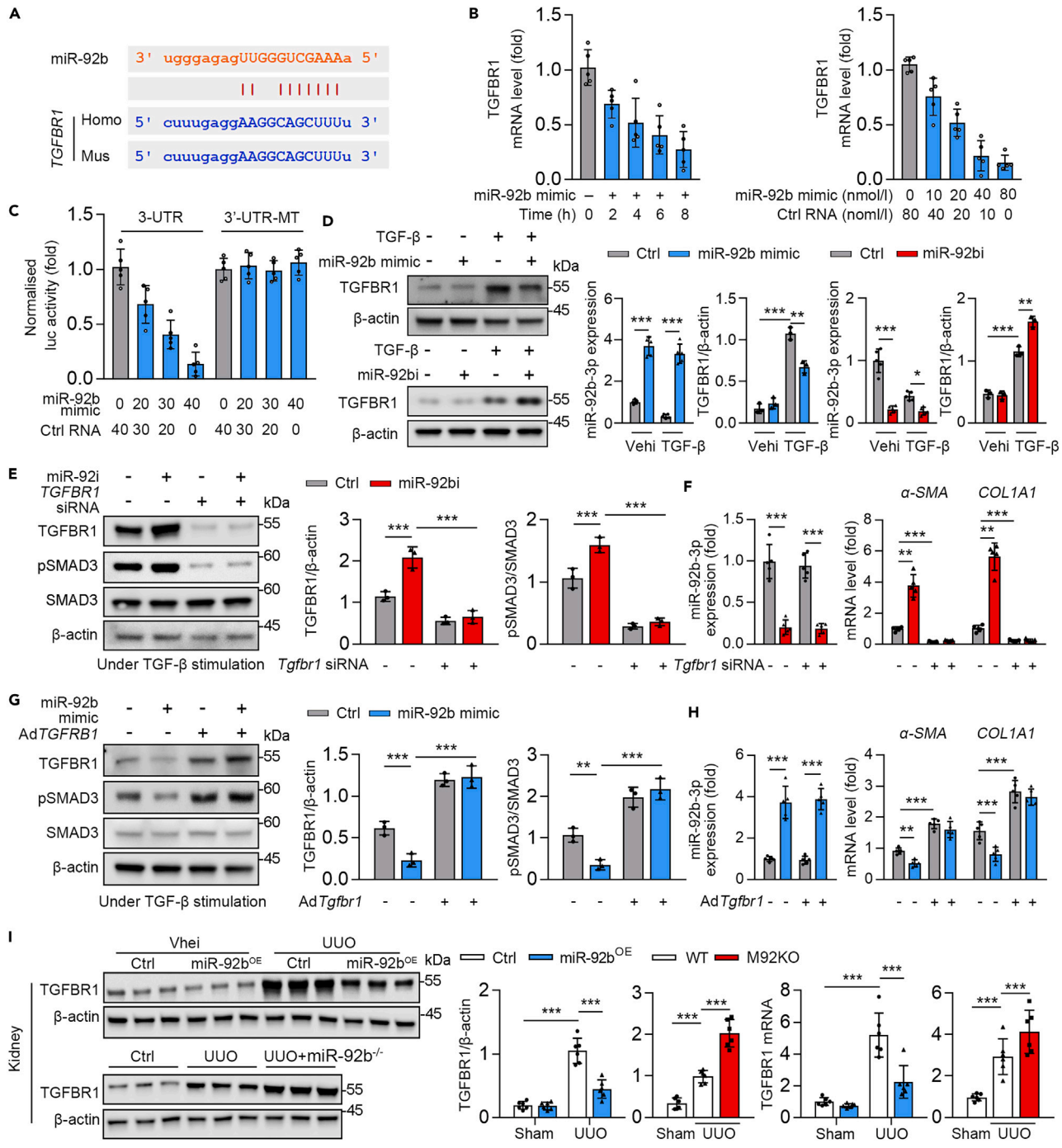

Figure 6. TGFBR1 is a direct target of miR-92b

(A) Graphical representation of the conserved miR-92b-3p binding motifs in the 3′-UTR of TGFBR1. Complementary sequences to the seed regions of miR-92b in the 3′-UTRs are conserved between the human (Homo) and mouse (Mus) sequences.

(B) HK2 cells were treated with miR-92b-3p mimic or control (Ctrl) RNA, and qPCR analysis was used to determine the mRNA level of TGFBR1; n = 5.

(C and D) (C) Luciferase (luc) activity of the reporter constructs containing either wild-type or mutated (MT) 3′-UTR of murine TGFBR1 after treatment of HK2 cells (n = 5), and (D) protein levels of TGFBR1 and β-actin in HK2 cells treated with miR-92b mimic (or miR-92b-3p inhibitor) or Ctrl RNA determined by western blotting (n = 3); quantitative results are shown in the right panel. qPCR analysis of miR-92b-3p (n = 5).

(E) Protein levels of TGFBR1, *p*-SMAD3, SMAD3, α-SMA, and β-actin HK2 cells treated with miR-92b inhibitor and/or *TGFBR1* siRNA determined by western blotting (n = 3); quantitative results are shown in the right panel.

(F) HK2 cells treated with or without *TGFBR1* siRNA. qPCR analysis of the expression of miR-92b-3p and the mRNA levels of *COLL1A1*, and *α-SMA*; n = 5.

Figure 6. *Continued*

(G) Protein levels of TGFBR1, *p*-SMAD3, SMAD3, α-SMA, and β-actin HK2 cells treated with miR-92b mimic and/or *TGFBR1* overexpressing adenovirus vector (Ad *TGFBR1*) determined by western blotting; n = 3; quantitative results are shown in the right panel.

(H) The qPCR analysis of the expression of miR-92b-3p and the mRNA levels of *COL1A1*, and *α-SMA* in HK2 cells treated with or without Ad *TGFBR1*; n = 5.

(I) Protein levels of TGFBR1 and β-actin, and mRNA levels of *Tgfbr1* in kidney tissue of miR-92b KO or miR-92b OE mice; n = 6. Data are expressed as means ± SD; *p < 0.05, **p < 0.01, ***p < 0.001.

DISCUSSION

In this study, we elucidated the mechanism linking miR-92b-3p and TGFBR1 in TGF-β-induced renal fibrosis. Altogether, our findings substantiate the involvement of miR-92b-3p in mediating TGF-β-induced EMT and renal fibrosis through the disruption of TGFBR1, which is physiologically significant in DKD. Moreover, our results indicated that miR-92b-3p overexpression reversed renal fibrosis in UUO mice. We identified miR-92b-3p as an important mediator of renal fibrosis.

Most studies on miR-92b-3p have focused on its role in cancer development. However, the relationship between miR-92b-3p expression and cancer development remains controversial.[28] Previous studies have suggested that miR-92b-3p expression is increased in most cancers, including colorectal cancer,[29] esophageal squamous cell cancer,[30] gastric cancer,[31] non-SCLC,[32] and clear cell renal cell carcinoma.[33] In contrast, miR-92b-3p has been confirmed as a tumor suppressor in pancreatic cancer[34] and triple-negative breast cancer.[35] This suggests that the biological functions of miR-92b-3p are tissue- and cell-specific. In the present study, we identified miR-92b-3p as a novel endogenous inhibitory factor of the TGF-β signaling pathway in the HK2 cells or HRFs (Figures 5 and S3). It repressed the TGF-β signaling pathway via directly inhibiting TGFBR1 expression (Figure 6). Consistent with our results, another study suggested that miR-92b-3p participates in TGF-β mediated EMT.[36] TGF-β2-induced circ-PRDM5 facilitated human lens epithelial cells migration, invasion, and EMT by adsorbing miR-92b-3p and increasing COL1A2 expression, offering new insights into the development of posterior capsule opacities.[36] The role of TGF-β in fibrosis and cancer is complex and sometimes contradictory, exhibiting either inhibitory or promoting effects depending on the stage of the disease.[37] The regulatory role of miR-92b on the TGF-β signaling pathway may be an important reason for the contradictory effects of mir-92b.

Interestingly, some studies have shown that SMAD7 is a direct target of miR-92b-3p.[38,39] SMAD7 is an intracellular antagonist for TGF-β signaling; it is known to associate with activated TGFBR1 and hinder the activation of receptor-regulated SMAD (R-SMAD) by preventing their interaction with activated TGFBR1 and consequent phosphorylation.[40,41] However, another study showed that suppression of miR-92b-3p expression decreased the gene and protein expression of SMAD7, BMP2, and RUNX-2, and inhibited BMSC proliferation and osteoblast differentiation, leading to aggravated osteoporosis.[42] In the current study, treatment with the miR-92b-3p mimic did not significantly regulate the mRNA level of SMAD7 in HK2 cells without TGF-β stimulation (Figure S4A). In line with this, SMAD7 was not upregulated in the kidneys of miR-92b KO mice compared to that in control mice (RNA-seq; Figure 4A). UUO resulted in progressive tubulointerstitial fibrosis associated with increased expression of TGF-β1 and *Smad7* mRNAs, activation of R-SMADs, expression of Smurf1 and Smurf2, and a significant decrease in SMAD7 protein level; the reduction of SMAD7 may also be caused by ubiquitin-dependent protein degradation.[43] Furthermore, we found that miR-92b-3p knockout and overexpression increased and decreased, respectively, the mRNA levels of SMAD7 in UUO mice (Figure S4B). In addition, miR-92b-3p mimic treatment decreased the mRNA levels of SMAD7 under TGF-β stimulation in a TGFRB1-dependent manner (SMAD7 is a downstream target of TGFBR1) (Figure S4C). Taken together, our data show that TGFBR1 but not SMAD7 is a direct target of miR-92b-3p in HK2 cells.

Our study illustrated that miR-92b-3p regulates renal fibrosis by directly targeting TGFBR1 and regulating TGF-β/Smad signaling in UUO- and uIRI-induced renal fibrosis. These findings provide novel insights into the pathogenesis of DKD and suggest that miR-92b-3p may be used as an effective therapeutic for DKD treatment.

Limitations of the study

First, we did not construct a tubular epithelial cell-specific miR-92b knockout model to observe its role in renal fibrosis. Second, since the proliferation of HRFs may participate in the pathogenesis of renal fibrosis, whether miR-92b-3p is also involved in the proliferation of HRFs warrants further study. Finally, although our study identified a mechanistic link between the induction of renal fibrosis by TGF-β via miR-92b-3p/TGFRB1 signaling in acute kidney injury model (UUO and 24 h after uIRI surgery), further research is needed to determine whether miR-92b-3p plays an anti-fibrotic role in mouse models of CKD, such as unilateral nephrectomy.

STAR★METHODS

Detailed methods are provided in the online version of this paper and include the following:

- KEY RESOURCES TABLE
- RESOURCE AVAILABILITY
  - Lead contact
  - Materials availability
  - Data and code availability
- EXPERIMENTAL MODEL AND STUDY PARTICIPANT DETAILS
  - Animal models

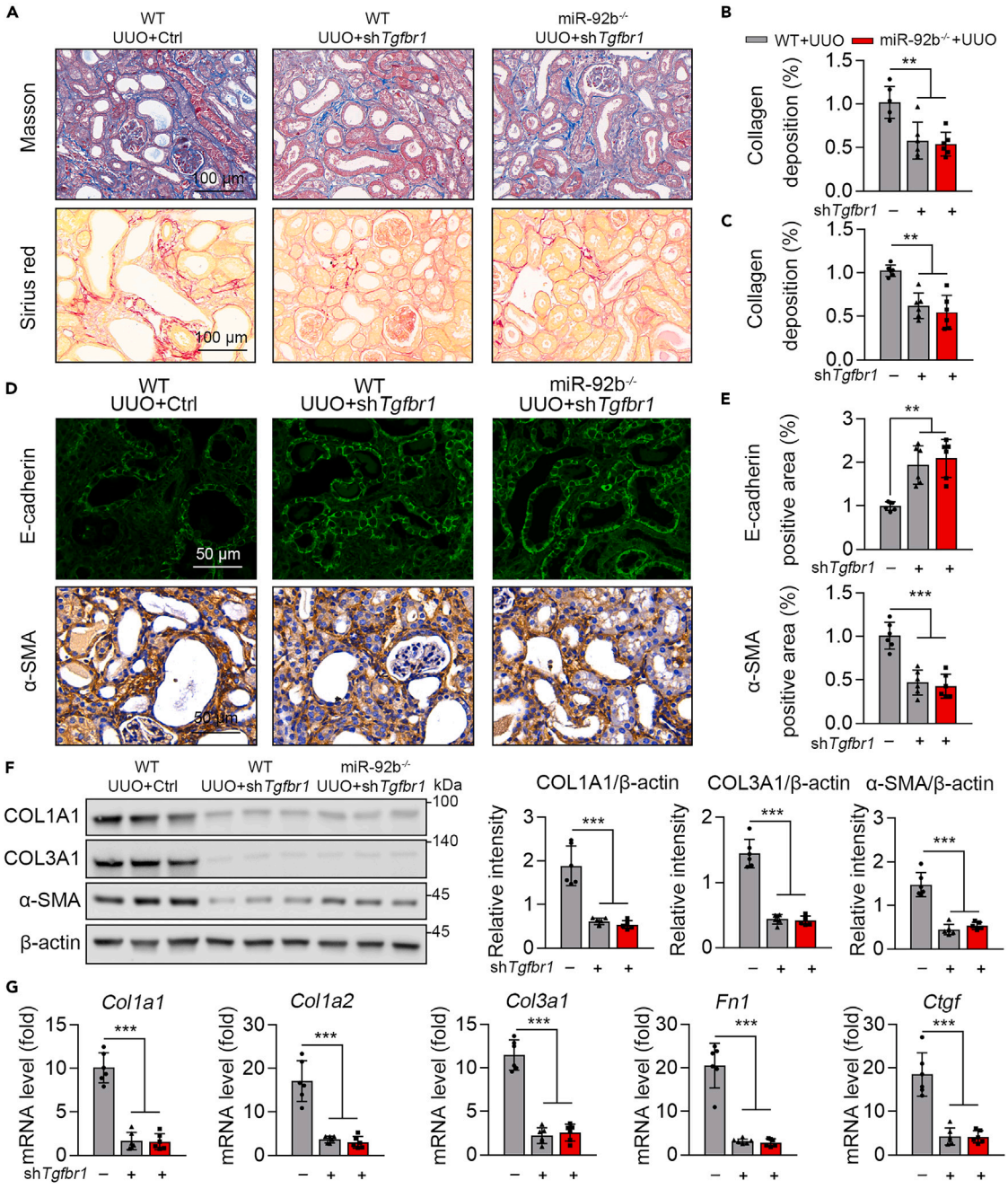

Figure 7. miR-92b targets TGFBR1 against renal fibrosis. WT or M92KO mice were transfected with AAV-Ctrl or AAV-sh*Tgfbr1* as indicated, sacrificed 7 days after UUO surgery, and kidney sections were collected

(A–C) Representative images of Masson's trichrome staining and Sirius red staining of kidney sections from mice (A); Scale bar: 100 μm. Quantitative analysis of fibrotic area as determined by Masson's trichrome staining (B) and Sirius red staining (C).

(D and E) Representative images of E-cadherin immunofluorescence staining and immunohistochemistry of α-SMA content in renal tissue (D), and quantitative analysis of positive area (E); Scale bar: 50 μm.

(F) Western blotting of COL1A1, COL3A1, α-SMA, and β-actin; quantitative results are shown in the right panel. β-actin was used as the loading control.

(G) qPCR analysis of the mRNA levels of *Col1a1*, *Col1a2*, *Col3a1*, *Fn1*, and *Ctgf*. Data are expressed as means ± SD; n = 6 per group; *p < 0.05, **p < 0.01, ***p < 0.001. Results from three independent experiments are presented.

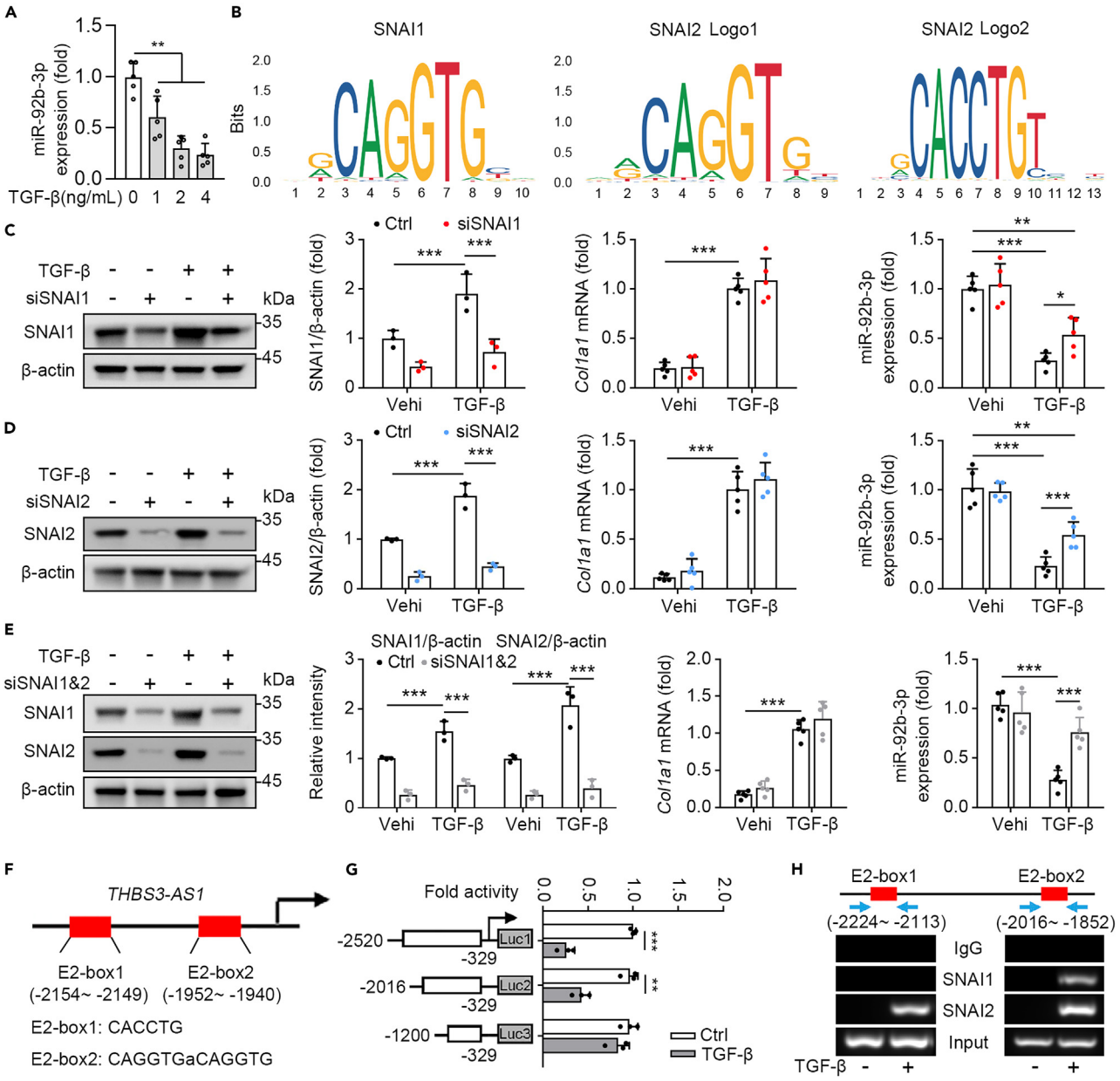

Figure 8. SNAI1 and SNAI2 inhibited miR-92b expression

(A) The expression of miR-92b-3p in HK2 cells treated with TGF-β for 12 h, as detected by qPCR, n = 5.

(B) Sequence logo of transcription factor SNAI1 and SNAI2.

(C–E) Protein levels of SNAI1, SNAI2, and β-actin in HK2 cells treated with SNAI1 siRNA (siSNAI1), SNAI2 siRNA (siSNAI2), or control siRNA as indicated in the figure, as detected by western blotting; quantitative results are shown; n = 3. Expression of *Col1a1* and miR-92b-3p as determined by qPCR; n = 5.

(F) Schematic representation of the human THBS3-AS1 promoters with the putative E2-box promoter shown as a red box.

(G) A series of truncated THBS3-AS1 promoters fused to the luciferase reporter gene was co-transfected into HEK293T cells under TGF-β stimulation together with the pcDNA3.1 Renilla plasmid (Ctrl). The relative luciferase activity was presented as folds of Ctrl (n = 3).

(H) DNA fragments containing the flanking region of the E2-box on the THBS3-AS1 promoters were immunoprecipitated with anti-SNAI1 or anti-SNAI2 antibodies. Data are expressed as means ± SD; n = 6 per group; *p < 0.05, **p < 0.01, ***p < 0.001. Similar results from three independent experiments are shown.

- ○ MiR-92b overexpression mice
- ○ TGFBR1 deficiency mice
- ○ Study approval

SUPPLEMENTAL INFORMATION

Supplemental information can be found online at https://doi.org/10.1016/j.isci.2023.108131.

ACKNOWLEDGMENTS

This work was supported by grants from the National Natural Science Foundation of China (82370876 to **S.Y.**, 82170842 and 82371572 to **Z.L.**, 82171556 to **L.K.**), Shenzhen Sustainable Development Science and Technology Special Project, China (No. KCXFZ20201221173600001 to **Z.L.**), Key Program Topics of Shenzhen Basic Research, China (No. JCYJ20220818102605013 to **L.K.**). Sequencing service was provided by Bioyi Biotechnology Co., Ltd. Wuhan, China.

AUTHOR CONTRIBUTIONS

Conceptualization, **S.Y.**; Methodology, **K.J.**, **L.L.**, and **J.X.**; Investigation, **G.Y.**; Writing – Original Draft, **Y.L.** and **S.Y.**; Writing –Review and Editing, **G.Y.** and **S.Y.**; Funding Acquisition, **S.Y.**, **L.K.**, and **Z.L.**; Resources, **L.K.** and **Z.L.**; Supervision, **S.Y.**, **L.K.**, and **Z.L**.

DECLARATION OF INTERESTS

The authors declare no competing interests.

Received: July 14, 2023
Revised: September 6, 2023
Accepted: September 30, 2023
Published: October 5, 2023

REFERENCES

1. Liu, Y. (2011). Cellular and molecular mechanisms of renal fibrosis. Nat. Rev. Nephrol. *7*, 684–696. https://doi.org/10.1038/nrneph.2011.149.
2. Eddy, A.A. (2000). Molecular basis of renal fibrosis. Pediatr. Nephrol. *15*, 290–301. https://doi.org/10.1007/s004670000461.
3. Sato, M., Muragaki, Y., Saika, S., Roberts, A.B., and Ooshima, A. (2003). Targeted disruption of TGF-beta1/Smad3 signaling protects against renal tubulointerstitial fibrosis induced by unilateral ureteral obstruction. J. Clin. Invest. *112*, 1486–1494. https://doi.org/10.1172/jci19270.
4. Nastase, M.V., Zeng-Brouwers, J., Wygrecka, M., and Schaefer, L. (2018). Targeting renal fibrosis: Mechanisms and drug delivery systems. Adv. Drug Deliv. Rev. *129*, 295–307. https://doi.org/10.1016/j.addr.2017.12.019.
5. Cho, N., Razipour, S.E., and McCain, M.L. (2018). Featured Article: TGF-β1 dominates extracellular matrix rigidity for inducing differentiation of human cardiac fibroblasts to myofibroblasts. Exp. Biol. Med. *243*, 601–612. https://doi.org/10.1177/1535370218761628.
6. Massagué, J. (2012). TGFβ signalling in context. Nat. Rev. Mol. Cell Biol. *13*, 616–630. https://doi.org/10.1038/nrm3434.
7. Meng, X.M., Nikolic-Paterson, D.J., and Lan, H.Y. (2016). TGF-β: the master regulator of fibrosis. Nat. Rev. Nephrol. *12*, 325–338. https://doi.org/10.1038/nrneph.2016.48.
8. Budi, E.H., Schaub, J.R., Decaris, M., Turner, S., and Derynck, R. (2021). TGF-β as a driver of fibrosis: physiological roles and therapeutic opportunities. J. Pathol. *254*, 358–373. https://doi.org/10.1002/path.5680.
9. Xavier, S., Vasko, R., Matsumoto, K., Zullo, J.A., Chen, R., Maizel, J., Chander, P.N., and Goligorsky, M.S. (2015). Curtailing endothelial TGF-β signaling is sufficient to reduce endothelial-mesenchymal transition and fibrosis in CKD. J. Am. Soc. Nephrol. *26*, 817–829. https://doi.org/10.1681/asn.2013101137.
10. Liang, J., Zhou, Y., Zhang, N., Wang, D., Cheng, X., Li, K., Huang, R., Lu, Y., Wang, H., Han, D., et al. (2021). The phosphorylation of the Smad2/3 linker region by nemo-like kinase regulates TGF-β signaling. J. Biol. Chem. *296*, 100512. https://doi.org/10.1016/j.jbc.2021.100512.
11. Cortez, M.A., Bueso-Ramos, C., Ferdin, J., Lopez-Berestein, G., Sood, A.K., and Calin, G.A. (2011). MicroRNAs in body fluids–the mix of hormones and biomarkers. Nat. Rev. Clin. Oncol. *8*, 467–477. https://doi.org/10.1038/nrclinonc.2011.76.
12. Weber, J.A., Baxter, D.H., Zhang, S., Huang, D.Y., Huang, K.H., Lee, M.J., Galas, D.J., and Wang, K. (2010). The microRNA spectrum in 12 body fluids. Clin. Chem. *56*, 1733–1741. https://doi.org/10.1373/clinchem.2010.147405.
13. Lai, E.C., Tomancak, P., Williams, R.W., and Rubin, G.M. (2003). Computational identification of Drosophila microRNA genes. Genome Biol. *4*, R42. https://doi.org/10.1186/gb-2003-4-7-r42.
14. Jiang, X., Tsitsiou, E., Herrick, S.E., and Lindsay, M.A. (2010). MicroRNAs and the regulation of fibrosis. FEBS J. *277*, 2015–2021. https://doi.org/10.1111/j.1742-4658.2010.07632.x.
15. Wei, Q., Mi, Q.S., and Dong, Z. (2013). The regulation and function of microRNAs in kidney diseases. IUBMB Life *65*, 602–614. https://doi.org/10.1002/iub.1174.
16. Chung, A.C.K., and Lan, H.Y. (2015). MicroRNAs in renal fibrosis. Front. Physiol. *6*, 50. https://doi.org/10.3389/fphys.2015.00050.
17. Suzuki, H.I. (2018). MicroRNA Control of TGF-β Signaling. Int. J. Mol. Sci. *19*, 1901. https://doi.org/10.3390/ijms19071901.
18. Kato, M., Zhang, J., Wang, M., Lanting, L., Yuan, H., Rossi, J.J., and Natarajan, R. (2007). MicroRNA-192 in diabetic kidney glomeruli

and its function in TGF-beta-induced collagen expression via inhibition of E-box repressors. Proc. Natl. Acad. Sci. USA *104*, 3432–3437. https://doi.org/10.1073/pnas.0611192104.

19. Wang, Q., Wang, Y., Minto, A.W., Wang, J., Shi, Q., Li, X., and Quigg, R.J. (2008). MicroRNA-377 is up-regulated and can lead to increased fibronectin production in diabetic nephropathy. FASEB J. *22*, 4126–4135. https://doi.org/10.1096/fj.08-112326.
20. Long, J., Wang, Y., Wang, W., Chang, B.H.J., and Danesh, F.R. (2010). Identification of microRNA-93 as a novel regulator of vascular endothelial growth factor in hyperglycemic conditions. J. Biol. Chem. *285*, 23457–23465. https://doi.org/10.1074/jbc.M110.136168.
21. Fu, Y., Zhang, Y., Wang, Z., Wang, L., Wei, X., Zhang, B., Wen, Z., Fang, H., Pang, Q., and Yi, F. (2010). Regulation of NADPH oxidase activity is associated with miRNA-25-mediated NOX4 expression in experimental diabetic nephropathy. Am. J. Nephrol. *32*, 581–589. https://doi.org/10.1159/000322105.
22. Huang, W., Ji, R., Ge, S., Zhou, D., Liu, Z., Sun, Y., Huang, W., and Lu, C. (2021). MicroRNA-92b-3p promotes the progression of liver fibrosis by targeting CREB3L2 through the JAK/STAT signaling pathway. Pathol. Res. Pract. *219*, 153367. https://doi.org/10.1016/j.prp.2021.153367.
23. Zhu, H.Y., Bai, W.D., Li, J., Tao, K., Wang, H.T., Yang, X.K., Liu, J.Q., Wang, Y.C., He, T., Xie, S.T., and Hu, D.H. (2016). Peroxisome proliferator-activated receptor-γ agonist troglitazone suppresses transforming growth factor-β1 signalling through miR-92b upregulation-inhibited Axl expression in human keloid fibroblasts in vitro. Am. J. Transl. Res. *8*, 3460–3470.
24. Leask, A. (2010). Potential therapeutic targets for cardiac fibrosis: TGFbeta, angiotensin, endothelin, CCN2, and PDGF, partners in fibroblast activation. Circ. Res. *106*, 1675–1680. https://doi.org/10.1161/circresaha.110.217737.
25. Derynck, R., and Zhang, Y.E. (2003). Smad-dependent and Smad-independent pathways in TGF-beta family signalling. Nature *425*, 577–584. https://doi.org/10.1038/nature02006.
26. Villarejo, A., Cortés-Cabrera, A., Molina-Ortíz, P., Portillo, F., and Cano, A. (2014). Differential role of Snail1 and Snail2 zinc fingers in E-cadherin repression and epithelial to mesenchymal transition. J. Biol. Chem. *289*, 930–941. https://doi.org/10.1074/jbc.M113.528026.
27. Guaita, S., Puig, I., Franci, C., Garrido, M., Dominguez, D., Batlle, E., Sancho, E., Dedhar, S., De Herreros, A.G., and Baulida, J. (2002). Snail induction of epithelial to mesenchymal transition in tumor cells is accompanied by MUC1 repression and ZEB1 expression. J. Biol. Chem. *277*, 39209–39216. https://doi.org/10.1074/jbc.M206400200.
28. Li, M., Shan, W., Hua, Y., Chao, F., Cui, Y., Lv, L., Dou, X., Bian, X., Zou, J., Li, H., and Lin, W. (2021). Exosomal miR-92b-3p Promotes Chemoresistance of Small Cell Lung Cancer Through the PTEN/AKT Pathway. Front. Cell Dev. Biol. *9*, 661602. https://doi.org/10.3389/fcell.2021.661602.
29. Gong, L., Ren, M., Lv, Z., Yang, Y., and Wang, Z. (2018). miR-92b-3p Promotes Colorectal Carcinoma Cell Proliferation, Invasion, and Migration by Inhibiting FBXW7 In Vitro and In Vivo. DNA Cell Biol. *37*, 501–511. https://doi.org/10.1089/dna.2017.4080.
30. Wang, W., Fu, S., Lin, X., Zheng, J., Pu, J., Gu, Y., Deng, W., Liu, Y., He, Z., Liang, W., and Wang, C. (2019). miR-92b-3p Functions As A Key Gene In Esophageal Squamous Cell Cancer As Determined By Co-Expression Analysis. OncoTargets Ther. *12*, 8339–8353. https://doi.org/10.2147/ott.S220823.
31. Li, C., Huo, B., Wang, Y., and Cheng, C. (2019). Downregulation of microRNA-92b-3p suppresses proliferation, migration, and invasion of gastric cancer SGC-7901 cells by targeting Homeobox D10. J. Cell. Biochem. *120*, 17405–17412. https://doi.org/10.1002/jcb.29005.
32. Lei, L., Huang, Y., and Gong, W. (2014). Inhibition of miR-92b suppresses nonsmall cell lung cancer cells growth and motility by targeting RECK. Mol. Cell. Biochem. *387*, 171–176. https://doi.org/10.1007/s11010-013-1882-5.
33. Wang, C., Uemura, M., Tomiyama, E., Matsushita, M., Koh, Y., Nakano, K., Hayashi, Y., Ishizuya, Y., Jingushi, K., Kato, T., et al. (2020). MicroRNA-92b-3p is a prognostic oncomiR that targets TSC1 in clear cell renal cell carcinoma. Cancer Sci. *111*, 1146–1155. https://doi.org/10.1111/cas.14325.
34. Long, M., Zhan, M., Xu, S., Yang, R., Chen, W., Zhang, S., Shi, Y., He, Q., Mohan, M., Liu, Q., and Wang, J. (2017). miR-92b-3p acts as a tumor suppressor by targeting Gabra3 in pancreatic cancer. Mol. Cancer *16*, 167. https://doi.org/10.1186/s12943-017-0723-7.
35. Li, Y.Y., Zheng, X.H., Deng, A.P., Wang, Y., Liu, J., Zhou, Q., Cheng, G.Y., and Jiang, Q. (2019). MiR-92b inhibited cells EMT by targeting Gabra3 and predicted prognosis of triple negative breast cancer patients. Eur. Rev. Med. Pharmacol. Sci. *23*, 10433–10442. https://doi.org/10.26355/eurrev_201912_19682.
36. Huang, P., Hu, Y., and Duan, Y. (2022). TGF-β2-induced circ-PRDM5 regulates migration, invasion, and EMT through the miR-92b-3p/COL1A2 pathway in human lens epithelial cells. J. Mol. Histol. *53*, 309–320. https://doi.org/10.1007/s10735-021-10053-7.
37. Peng, D., Fu, M., Wang, M., Wei, Y., and Wei, X. (2022). Targeting TGF-β signal transduction for fibrosis and cancer therapy. Mol. Cancer *21*, 104. https://doi.org/10.1186/s12943-022-01569-x.
38. Bu, F.T., Zhu, Y., Chen, X., Wang, A., Zhang, Y.F., You, H.M., Yang, Y.R., Yang, Y., Huang, C., and Li, J. (2021). Circular RNA circPSD3 alleviates hepatic fibrogenesis by regulating the miR-92b-3p/Smad7 axis. Molecular therapy. Nucleic acids *23*, 847–862. https://doi.org/10.1016/j.omtn.2021.01.007.
39. Wang, L.P., Geng, J.N., Sun, B., Sun, C.B., Shi, Y., and Yu, X.Y. (2020). MiR-92b-3p is Induced by Advanced Glycation End Products and Involved in the Pathogenesis of Diabetic Nephropathy. Evid. Based. Complement. Alternat. Med. *2020*, 6050874. https://doi.org/10.1155/2020/6050874.
40. Massagué, J. (2000). How cells read TGF-beta signals. Nat. Rev. Mol. Cell Biol. *1*, 169–178. https://doi.org/10.1038/35043051.
41. Wrana, J.L. (2000). Regulation of Smad activity. Cell *100*, 189–192. https://doi.org/10.1016/s0092-8674(00)81556-1.
42. Zhang, Y., Liu, M.W., He, Y., Deng, N., Chen, Y., Huang, J., and Xie, W. (2020). Protective effect of resveratrol on estrogen deficiency-induced osteoporosis though attenuating NADPH oxidase 4/nuclear factor kappa B pathway by increasing miR-92b-3p expression. Int. J. Immunopathol. Pharmacol. *34*, 2058738420941762. https://doi.org/10.1177/2058738420941762.
43. Fukasawa, H., Yamamoto, T., Togawa, A., Ohashi, N., Fujigaki, Y., Oda, T., Uchida, C., Kitagawa, K., Hattori, T., Suzuki, S., et al. (2004). Down-regulation of Smad7 expression by ubiquitin-dependent degradation contributes to renal fibrosis in obstructive nephropathy in mice. Proc. Natl. Acad. Sci. USA *101*, 8687–8692. https://doi.org/10.1073/pnas.0400035101.

STAR★METHODS

KEY RESOURCES TABLE

REAGENT or RESOURCE	SOURCE	IDENTIFIER
Antibodies		
a-SMA(1:100)	Proteintech	Cat#14395-1-AP; RRID:AB_2223009
E-cadherin(1:100)	Proteintech	Cat# 20874-1-AP; RRID:AB_10697811
a-SMA(1:1000)	Abcam	Cat#ab7817; RRID:AB_262054
CTGF (1:1000)	Abcam	Cat# ab6992; RRID:AB_305688
SMAD3(1:1000)	Abcam	Cat# ab40854; RRID:AB_777979
Histone H3 (1:1000)	Abcam	Cat# ab1791; RRID:AB_302613
b-actin(1:1000)	Abcam	Cat# ab8226; RRID:AB_306371
TGFβR1 (1:1000)	Abcam	Cat# ab235578
SNAI1 (1:1000)	Abcam	Cat# ab216347; RRID:AB_2910593
SNAI2 (1:1000)	Abcam	Cat# ab27568; RRID:AB_777968
COL1A1 (1:1000)	Novus	Cat# sc-293182; RRID:AB_2797597
COL3A1 (1:1000)	Novus	Cat# sc-514601
E-cadherin (1:1000)	Proteintech	Cat# #20874-1-AP; RRID: AB_10697811
p-SMAD3 (1:1000)	Thermo Fisher Scientific	Cat# 44-246G; RRID:AB_1502060
Goat anti-Rabbit IgG (H + L) Cross-Adsorbed Secondary Antibody, Alexa Fluor 488 (1:400)	invitrogen	Cat# A-11008; RRID:AB_143165
Chemicals, peptides, and recombinant proteins		
TGF-β1	PeproTech	Cat# 100-21
Cocktail	Roche	Cat# 04693132001
Trizol	invitrogen	Cat# 15596-026
Experimental models: Cell lines		
Human: HK-2	ATCC	Cat#CRL-2190
Human: HRGECs	ScienCell	Cat#4000
Human: HMCs	ScienCell	Cat#4200
Human:HRF	Procell	Cat#CP-H072
Human:HEK-293T	Procell	Cat#CL-0005
Oligonucleotides		
Primers for qPCR, see Table S1	This paper	N/A
TGFBR1 siRNA	Santa Cruz biotechnology	Cat# sc-40222
SNAI1 siRNA	Santa Cruz biotechnology	Cat# sc-38398
SNAI2 siRNA	Santa Cruz biotechnology	Cat# sc-38393
Control siRNA	Santa Cruz biotechnology	Cat #sc-37007
Experimental models: Organisms/strains		
Mouse: C57BL/6JGpt- MiR-92b^{em22Cd549}/Gpt	Gempharmatech Co., Ltd	N/A
Mouse: C57BL/6JGpt	Gempharmatech Co., Ltd	N/A
Recombinant DNA		
CV232 empty vector	GeneChemCompany	N/A
CV232 MiR-92b	GeneChemCompany	N/A
GV138 empty vector	GeneChemCompany	N/A
GV138 TGFBR1	GeneChemCompany	N/A

(*Continued on next page*)

Continued		
REAGENT or RESOURCE	SOURCE	IDENTIFIER
CV774 shTgfbr1	GeneChemCompany	N/A
CV774 empty vector	GeneChemCompany	N/A
Software and algorithms		
ImageJ	National Institutes of Health	https://ImageJ.nih.gov/ij/
GraphPad Prism 7.4	GraphPad	https://www.graphpad.com/
Adobe Photoshop CS6	Adobe	https://www.adobe.com/cn
Critical commercial assays		
Modified Sirius Red Stain Kit	Solarbio Life Science	Cat#G1472
Extraction Reagents kit	Solarbio Life Science	Cat# R0010
Rapid Gold BCA Protein Assay Kit	Thermo fisher scientific	Cat# A53225
Chemistar™ High-sig ECL Western Blotting Substrate	Tanon	Cat# 180-5001
miRNeasy Kit	Qiagen	Cat#217061
Universal cDNA synthesis kit	Roche	Cat# 11483188001
SYBR Green I master	Roche	Cat#04913914001
iScript cDNA Synthesis Kit	Bio-Rad	Cat#1708890
Immunohistochemistry kit	ZSGB-BIO	Cat#PV9001; PV9002; PV9000
Nuclear Protein Isolation Kit	Thermo Fisher Scientific	Cat# 78833
Deposited data		
Raw and analyzed data	This paper	GEO: GSE242295

RESOURCE AVAILABILITY

Lead contact

Further information and requests for resources and reagents should be directed to and will be fulfilled by the Lead Contact, Zhen Liang (liang.zhen@szhsopital.com).

Materials availability

This study did not generate new unique reagents.

Data and code availability

- Any additional information required to reanalyse the data reported in this paper is available from the lead contact upon request.
- This paper does not report original code
- The sequencing data reported in this paper are deposited in NCBI Gene Expression Omnibus (GEO) database with accession number GEO: GSE242295 and will be publicly available as of the date of publication. Accession numbers are listed in the key resources table.

EXPERIMENTAL MODEL AND STUDY PARTICIPANT DETAILS

Animal models

MiR-92b global knockout mice (miR-92b$^{-/-}$) (C57BL/6JGpt- Mir-92b^{em22Cd549}/Gpt; Strain ID: T050823) were purchased from Gempharmatech Co. Ltd (Jiangsu, Nanjing, China). We determined the sample size for our animal studies based on a comprehensive analysis of previously published research or preliminary studies. No mice were excluded from the statistical analysis. The mice were housed in specific pathogen-free (SPF) units at the Animal Center of Shenzhen People's Hospital, where they were maintained under controlled conditions. These conditions included a 12-hour light cycle (from 8 a.m. to 8 p.m.) at a temperature of 23 $\pm$ 1°C and 60–70% humidity. The mice had *ad libitum* access to a standard rodent diet and water provided in plastic bottles. Before the experiments, the mice were given a minimum of 7 days to acclimate to their housing environment. In each plastic cage, up to five mice were housed together with corn cob bedding material for comfort. Throughout the study, the mice were treated in a blinded manner, and randomization was performed prior to treatment administration. At the conclusion of the experiment, all mice were humanely euthanized in a CO_2 chamber, and blood and kidney samples were collected for further analysis.

Eight-week-old male C57BL/6J or miR-92b $^{-/-}$ mice were randomly assigned to either the sham surgery group or the unilateral ureteral obstruction (UUO) surgery group. The surgery was performed following a well-established protocol. Briefly, the mice were given general anesthesia via intraperitoneal administration of pentobarbital (50 mg/kg) prior to surgery. A left-sided incision was made to expose the left ureter, which was then double ligated with 6-0 silk. Kidneys subjected to ureter ligation, serving as nonfibrotic controls, were collected at the designated time points (7 days or 10 days) after surgery. To induce unilateral ischemia-reperfusion injury (uIRI), the left renal artery was exposed through a left abdominal incision and clamped with a vascular clamp for 45 minutes. After 45 minutes, the clamp was released, and the left kidney returned to a bright red color from its initial dark red, indicating successful modeling. During the uIRI surgery, mice were kept on a heating pad to maintain their body temperature at 37°C. The injured kidney and the contralateral kidney were collected at the designated time points after surgery for further analysis.

MiR-92b overexpression mice

Eight-week-old C57BL/6J mice received *in situ* renal injection with AAV9-*Ctrl* (control group) or AAV9-*Ggt*-miR-92b (miR-92b overexpression group; *Ggt*, proximal tubule specific promoter) (n = 6). Adeno-associated virus type 9 constructs including the CV232 empty vector and miR-92b (2.37 E + 13 v.g./ml) were provided by GeneChem Company (Shanghai, China). After two weeks of infection by AAV, the mice received UUO or uIRI surgery, as mentioned before.

TGFBR1 deficiency mice

Eight-week-old miR-92b$^{-/-}$ mice received *in situ* renal injection with AAV9-*Ctrl* (control group) or AAV9-*Ggt-shTgfbr1* (TGFBR1 deficiency group; *Ggt*, proximal tubule specific promoter) (n = 6). Adeno-associated virus type 9 constructs including the CV774 empty vector and *shTgfbr1* (6.25 E + 13 v.g./ml) were provided by GeneChem Company (Shanghai, China). After two weeks of infection by AAV, the mice received UUO, as mentioned before.

Study approval

All animal care and experimental protocols for *in vivo* studies conformed to the Guide for the Care and Use of Laboratory Animals, published by the National Institutes of Health (NIH; NIH publication no.: 85–23, revised 1996), was approved by the Animal Care Committees of Jinan University (The ethics approval number: 20210303-52), and were performed in compliance with the ARRIVE guidelines.

Cell culture and transfection

The cell lines human proximal tubular epithelial cells (HK2 cells) (Cat. #CRL-2190), were purchased from American Type Culture Collection (Manassas, VA, USA) and maintained in Minimum Essential Medium (Thermo Fisher Scientific, Shanghai, China; Cat. #10373017). Human renal glomerular endothelial cells (HRGECs) (ScienCell, Carlsbad, CA, USA; Cat. #4000) were cultured in Endothelial Cell Medium (ScienCell, Cat.#1001) and human mesangial mells (HMCs) (ScienCell, Cat. #4200) were cultured in Mesangial Cell Medium (ScienCell, Cat. #4201). Human renal fibroblasts (HRF) (Procell Life Science&Technology, Wuhan, china; Cat. #CP-H072) were cultured in human kidney fibroblast complete culture medium (Procell, Cat. #CM-H072) and HEK-293T (Procell, Cat. #CL-0005) in Dulbecco's Modified Eagle's Medium (Procell, Cat. #PM150210). Cells were regularly checked for mycoplasma in a standardised manner, by a qPCR test, performed under ISO17025 accreditation to ensure work was conducted in mycoplasma-negative cells. All kinds of media were supplemented with 10% FBS (Gibco, Grand Island, NY), 100 U·mL−1 of penicillin (Gibco), and 100 mg·mL−1 of streptomycin (Gibco). All cells were cultured in a 37°C incubator containing 5% CO_2.

The miR-92b-3p mimic was a duplex RNA with the sense sequence 5′-UAUUGCACUCGUCCCGGCCUCC-3′ and antisense sequence 5′-AGGCCGGGACGAGUGCAAUAUU-3′. Non-targeting negative control sequences (sense: 5′-UUCUCCGAACGUGUCACGUTT-3′ and antisense: 5′-ACGUGACACGUUCGGAGAATT-3′were used as controls. The inhibitor of miR-92b-3p (5′-GGAGGCCGGGACGAGUGCAAUA-3′) is a single RNA sequence complementary to miR-92b-3p. A non-targeting negative control sequence (5′-CAGUACUUUUGUGUAGUA CAA-3′) was used as the control. Targeted siRNAs against Tgfbr1 and non-targeting control siRNAs were purchased from Santa Cruz Biotechnology (Dallas, TX, USA). Transient transfections were performed using Lipofectamine 3000 (Invitrogen) according to the manufacturer's instructions. Briefly, the cells were plated at a density of 5 × 10^4 cells/well and cultured for 24 h. siRNA or non-targeting control siRNA were transfected at a final concentration of 50 pmol·mL−1 using lipofectamine. After 6 h, the culture medium was replaced with fresh growth medium. Knockdown effectiveness was determined by western blotting.

METHOD DETAILS

Kidney pathology assessment

Masson's trichrome-stained and Sirius red-stained samples from the kidney was examined to assess collagen deposition. All image analyses were conducted using Photoshop CS6 (Adobe Systems Software Ireland Ltd). Immunohistochemistry analysis was performed using a kit from ZSGB-BIO (Beijing, China; Cat. No. PV9001 & PV9002). Paraffin sections were subjected to a dewaxing reagent (Solarbio, Cat. No. YA0031) followed by a series of ethanol washes (anhydrous ethanol, 95% ethanol, and 75% ethanol). Excess liquid was removed, and the sections were then washed with distilled water for 1 minute before being placed in PBS buffer. Antigen retrieval was performed using citric acid buffer. To block endogenous peroxidase activity, an appropriate amount of blocker was added and incubated at room temperature for 10 minutes. The

samples were then washed three times with PBS buffer for 3 minutes each. Next, an appropriate amount of primary antibody was added based on tissue size, and the samples were incubated overnight at 4°C. After incubation, the samples were rinsed three times with PBS buffer for 3 minutes each. To enhance the reaction, an appropriate amount of reaction enhancement solution was added, and the samples were incubated at 37°C for 20 minutes. The samples were then rinsed three times with PBS buffer for 3 minutes each. Subsequently, an enhanced enzyme-conjugated goat anti-mouse IgG polymer was added, and the samples were incubated at 37°C for 20 minutes. After incubation, the samples were rinsed three times with PBS buffer for 3 minutes each. DAB color solution was added and incubated at room temperature for 5–8 minutes. The samples were then rinsed with running water and counterstained with hematoxylin. Following dehydration and transparency, the slides were sealed with Rhamsan gum (Servicebio, Cat# WG10004160). Positive sites were analyzed using Photoshop CS6 (Adobe Systems Software Ireland Ltd). Please assist me with proofreading and plagiarism reduction.

Immunofluorescent staining

Kidney tissues were embedded in paraffin and sliced into 4-μm-thick sections. Following a 30-minute blocking step with goat serum, the tissues were incubated overnight at 4°C with primary antibodies targeting E-cadherin (1:100, Proteintech, Cat. #20874-1-AP). As secondary antibodies, Alexa Fluor goat antibodies against murine IgG (Invitrogen, Carlsbad, USA; Cat. #A-11008) were used. Negative controls were established by substituting the primary antibodies with nonimmune serum from the same species. Subsequently, the samples were counterstained with DAPI (1:1000 dilution) for 15 minutes. All sections were examined using a Laica microscope (Wetzlar, Germany).

Protein extraction and western blot analysis

Renal tissue or cell samples were lysed on ice in lysis buffer containing a cocktail of proteinase inhibitors and protein phosphatase inhibitors (Solarbio Life Science). The extracted protein concentrations were quantified using a Rapid Gold BCA Protein Assay Kit (Thermo Fisher, Shanghai, China), mixed with loading buffer, and boiled. Proteins were resolved on 12% SDS-PAGE in running buffer. The separated proteins were transferred to polyvinylidene difluoride (PVDF) membranes (Bio-Rad), blocked with blocking buffer, and incubated at 4°C overnight with the following primary antibodies: β-actin (Cat. #ab8226), CTGF (Cat. #ab ab6992), α-SMA (Cat. #ab7817), SMAD3 (Cat. #ab40854), H3 (Cat. #ab1791), TGFβR1 (Cat. #ab235578), SNAI1 (Cat. #ab216347) and SNAI2 (Cat. #ab27568) (all from Abcam, Cambridge, MA, USA), COL1A1 (Cat. #sc-293182), COL3A1 (Cat. #sc-514601), E-cadherin (Cat. sc-8426; Novus, Ontario, Canada), phosphor-SMAD3 (Ser423, Ser425; Cat. #44-246G; Thermo Fisher Scientific, MA, USA). The blots were then washed and incubated with secondary antibodies. After washing three times with TBST, signals were detected using chemiluminescence (Tanon, Shanghai, China). The density of the immunoreactive bands was analyzed using the Image J software.

Quantitative real-time PCR

miRNA was extracted using the miRNeasy Kit (Qiagen), followed by Universal cDNA synthesis kit (Roche). LNA PCR primer set, mature miR-92b-3p was purchased from Tsingke, Beijing, China. The cDNA was analysed by quantitative PCR with SYBR Green I master (Roche) on a LightCycler 480 (Roche) and U6 small RNA was used for data normalization, followed by the operation steps: 95°C for 20 s, 44 cycles of 95°C for 10 s, 60°C for 20 s, and 72°C for 25 s. Data are represented using the ΔΔCt method. The primers used for quantitative qPCR were as follows: 1) mouse miR-92b-3p primers24: forward 5′-gtccgctattgcactcgtcccggcctcc-3′ and reverse 5′-gtgcgtgtcgtggagtc-3′; 2) human miR-92b-3p primers25: forward 5′-tattg cactcgtcccggcctcc-3′and revers 5′-tggtgtcgtggagtcg-3′; 3) U6 primers: forward: 5′-gtccgcgtgctcgcttcggcagc-3′ and reverse 5′-gtgcgtgtcgtg gagtc-3′.

Total RNA was extracted from cells or tissues using the TRIzol reagent (Invitrogen). First-strand cDNA was synthesized from 1 μg total RNA using the iScript cDNA Synthesis Kit (Bio-Rad, Hercules, USA). The relative amount of each mRNA was quantified using quantitative PCR (qPCR) using the Eppendorf RealPlex 4 qPCR Real Time ThermoCycler (Eppendorf, Hamburg, Germany), and mRNA expression was normalized against β-actin mRNA expression. The primer sequences are listed in Table S1. The $2^{-\Delta\Delta ct}$ algorithm was used for qPCR analysis.

Dual-luciferase reporter assay

The cells were transfected with a p3TP-Luc reporter plasmid containing PAI-1 promoter elements using the Effectene transfection reagent (QIAGEN, Germany) as per the manufacturer's instructions. Transfection efficiency was determined by co-transfection with the β-gal reporter plasmid. The transfection mixture was removed 24 h later and the medium was replaced with fresh medium with or without the miR-92b mimic. Luciferase and galactosidase activities were measured after 24 h. All assays were performed in triplicates.

Isolation of nuclear protein

Cell nuclear fractions were separated using the NE-PER Nuclear and Cytoplasmic Extraction Reagents kit (Thermo Scientific, Cat. No 78833). In short, vortex the tube vigorously on the highest setting for 15 seconds to fully suspend the cell pellet (or Tissues were homogenized in PBS). Incubate the tube on ice for 10 min. Next, add ice-cold CER II to the tube. Then, vortex the tube and incubate tube on ice. Centrifuge the tube for 5 min at maximum speed in a microcentrifuge (~16,000 g), and transfer the supernatant (cytoplasmic extract) to a tube. As for suspend the insoluble (pellet) fraction, which contains nuclei, in ice-cold NER, and then vortex on the highest setting for 15 seconds. Place the sample on ice and continue vortexing for 15 seconds every 10 min, for a total of 40 min. Centrifuge the tube at maximum speed (~16,000 g) in a microcentrifuge for 10 min, and transfer the supernatant (nuclear extract) fraction to a tube.

Prediction of transcription factors

JASPAR (http://jaspar.genereg.net/) is an open-access database containing manually curated, non-redundant transcription factor (TF) binding profiles for TFs across six taxonomic groups. The promoter region of the target gene was obtained from UCSC (http://genome.ucsc.edu/).

QUANTIFICATION AND STATISTICAL ANALYSIS

All data were generated from at least three independent experiments. Each value was presented as the mean ± SD. All raw data were initially subjected to a normal distribution and analysis by one-sample Kolmogorov-Smirnov (K-S) nonparametric test using SPSS 22.0 software. For animal and cellular experiments, a two-tailed unpaired Student's *t* test was performed to compare two groups. One-way ANOVA followed by the Bonferroni's post-hoc test was used to compare more than two groups. The correlation coefficient was calculated using Spearman's correlation test. To avoid bias, all statistical analyses were performed blindly. Statistical significance was indicated at $*p < 0.05$, $**p < 0.01$, and $***p < 0.001$.